Molecular dynamics of collision cascades with composite pair–many-body potentials

S. P. Chou and N. M. Ghoniem
Mechanical, Aerospace, and Nuclear Engineering Department, University of California Los Angeles, Los Angeles, California 90024-1597
(Received 28 June 1990)

An empirical, composite interatomic potential is developed to describe interaction of energetic particles by pair potentials at high energies and many-body potentials at low energies. Molecular-dynamics studies of low-energy collision cascades are performed. The displacement threshold surface in copper is investigated and compared to experimental data. Our computer simulations show good agreement with the experimental results of King and Benedek at 10 K.

I. INTRODUCTION

Pair-interaction potentials for the description of collision-cascade dynamics have been widely used to investigate the transport of ions in solids and the generation of atomic displacements. Satisfactory results have been achieved by using numerical simulation techniques such as the Monte Carlo and molecular-dynamics (MD) methods.[1–14] Displacement threshold energies, however, are generally in the range of few times the lattice binding energy. Therefore, many-body effects are expected to be important in the sub- to tens of eV range where pair potentials do not provide an accurate description of atomic interactions. Furthermore, the many-body interaction of atoms at low energy can affect the morphology of the collision cascade because its range of influence is greater than that of pure pair potentials. Therefore, in order to accurately treat cascade dynamics, it is necessary to develop a more realistic treatment of atomic interactions at low energies. A simple many-body potential based on the embedded-atom method (EAM) is used in this work.[15–18]

At high incident-ion energies, the interaction between the incident ion and a stationary one is primarily that of a pair-interaction type. As the kinetic energy decreases, the effects of the surrounding lattice become more significant and the interaction must contain many-body (local) contributions.

The EAM approach has been successfully applied to a variety of problems where the solid is very near its equilibrium configuration. However, the method is not *ab initio,* but rather, can be viewed as a phenomenological approach that is based on the density-functional theory. The Hohenberg-Kohn theorem[19] states that the total energy $E[\rho(r)]$ is a functional of the electron density $\rho(r)$. The exact form of the functional dependence is not unique, and empirical approaches must be followed to determine constants associated with the assumed form. Although simpler approaches to the determination of the embedding functional and associated constants have recently been reported in the literature,[20,21] we will use the EAM approach as originally developed by Daw and Baskes[15,16] and the approximations of Foiles.[17] It is recognized that the many-body contributions to the potential are reasonably well represented by the EAM. However, the atomic displacement process requires further knowledge of the potential at atomic separation distances that are shorter than the range of EAM applicability. In Sec. II, we describe an empirical method to determine a suitable composite potential for copper that covers all ranges of interatomic distances. The computational method is then described in Sec. III. Results of cascade simulation in copper are given in Sec. IV, and conclusions follow in Sec. V.

II. COMPOSITE POTENTIAL

In order to treat the atomic interaction in a continuous manner, a potential that preserves the nature of established interatomic potentials at the two energy extremes must be used. In our approach, Ziegler's pair potential[22] is selected to describe the atomic interactions at the high-energy end and an approximation to the EAM many-body potential at the low-energy end. For the transition region, a cubic-spline potential is used which allows continuity of this composite potential throughout the entire energy range. The high-energy pair potential is represented by Ziegler *et al.*[22] in the form

$$\phi_Z(R_{ij})=\frac{Z_iZ_je^2}{R_{ij}}\sum_{k=1}^{4}c_k e^{-b_kR_{ij}/a_0}\,, \tag{1}$$

where Z_i and Z_j are the atomic numbers of the interacting particles i and j, respectively, and R_{ij} is the separation distance between them, e is the electron charge, c_k and b_k are constants, and a_0 is the screening length.[22]

The approximate many-body EAM potential is derived by Foiles,[17] based on the EAM framework originally developed by Daw *et al.*,[15,16] and it has the form

$$\phi_{\rm EAM}(R_{ij})=\phi_{ij}(R_{ij})+2\frac{\partial F_i(\bar\rho^{\,a})}{\partial\rho}\rho_{ij}^a(R_{ij})+\frac{\partial^2F_i(\bar\rho^{\,a})}{\partial\rho^2}[\rho_{ij}^a(R_{ij})]^2\,, \tag{2}$$

where F_i is the embedding function for atom i, $\rho_{ij}^a(R_{ij})$ is the *average* local electron-density contribution from atom j on atom i at a separation distance of R_{ij}, ϕ_{ij} is the core-core pair repulsive potential between interacting

atoms i and j, and $\bar{\rho}^a$ is the total average local background electron density from all of the neighboring atoms on atom i.

A transitional cubic-spline potential which bridges the Ziegler and EAM potentials is assumed as

$$\phi_s(R_{ij}) = \sum_{k=0}^{3} d_k R_{ij}^k , \tag{3}$$

where d_k are splining constants. This assumed spline potential satisfies the following constrains:

$$\phi_Z(R_{ij})|_{R_{ij}=r_1} = \phi_s(R_{ij})|_{R_{ij}=r_1} ,$$

$$\phi_{\mathrm{EAM}}(R_{ij})|_{R_{ij}=r_2} = \phi_s(R_{ij})|_{R_{ij}=r_2} ,$$

$$\left.\frac{\partial \phi_Z(R_{ij})}{\partial R_{ij}}\right|_{R_{ij}=r_1} = \left.\frac{\partial \phi_s(R_{ij})}{\partial R_{ij}}\right|_{R_{ij}=r_1} ,$$

$$\left.\frac{\partial \phi_{\mathrm{EAM}}(R_{ij})}{\partial R_{ij}}\right|_{R_{ij}=r_2} = \left.\frac{\partial \phi_s(R_{ij})}{\partial R_{ij}}\right|_{R_{ij}=r_2} .$$

The interatomic potential and force are thus continuous functions of the interatomic separation distance. The values of r_1 and r_2 are chosen so as to reduce drastic force variations when a particle moves from one potential regime to another. This is very critical because the force for the cubic-spline potential is only piecewise continuous. A proper selection of r_1 and r_2 can reduce the degree of discontinuity in force derivatives at these parametric distances. The interaction of two lattice atoms at a separation r is completely described by the composite potential of the form:

$$\phi(R_{ij}) = \begin{cases} \phi_Z(R_{ij}), & 0 < R_{ij} \le r_1 , \\ \phi_S(R_{ij}), & r_1 \le R_{ij} \le r_2 , \\ \phi_{\mathrm{EAM}}(R_{ij}), & r_2 \le R_{ij} \le r_c , \end{cases}$$

where r_c is the cutoff distance ($\sim$5.0 Å) for the low-energy many-body potential. It is worth mentioning that this spline potential is flexible enough for extensions to other combinations of high-energy pair potentials and of low-energy many-body potentials. Possible candidates for high-energy pair interactions are the Moliere and Kr-C potentials.[22] The distances r_1 and r_2 are chosen to be 1.5 and 2.0 Å, respectively. The spline potential is not only a function of the interatomic separation, but is also a function of the total average local electron density. For instance, in sputtering simulations, near-surface atoms sit in different total average local electron densities than atoms in the bulk because of their neighboring atom configurations.

Table I gives a typical set of fitting parameters d_k for equilibrium lattice atoms in bulk copper. The total average local electron density $\bar{\rho}^a$ is 0.0276 Å^{-3}. The local electron density for copper with an FCC structure is based on the quantum-mechanical wave functions of Clementi and Roetti,[23] and the embedding function for copper is derived from the work of Foiles *et al.*[18]

Figure 1 shows plots of the composite potential as a function of the interatomic separation, and at total average local electron densities of 0.02, 0.0276, and 0.03 Å^{-3}.

TABLE I. Spline-potential parameters for equilibrium local electron density.

Index, k	d_k
0	60.559
1	119.58
2	−162.68
3	61.414

III. COMPUTATIONAL METHOD

Because of computational constraints (e.g., the computer memory size and its speed, computing cost, and the desired turnaround time), the MD technique can only simulate a small ensemble of atoms. It is important, therefore, to develop appropriate boundary conditions so that simulation results are nearly size independent. The energy introduced by the primary knock-on atom (PKA) must be accurately dissipated in the form of atomic displacements and at the computational cell boundaries. If rigid boundaries are used, reflective energy exchange with the rigid boundaries is likely to influence subsequent dynamics.

A new MD computer code CASC-MD has been developed to study low-energy collision cascades. With this code, appropriate energy dissipation to below $\sim$1 eV is ensured in the following ways.

(1) The computational cell size is varied to show that the collisional phase of the cascade dynamics is accurately represented.

(2) Two extra atomic planes are added to the computational box in the form of special viscoelastic "boundary" atoms; thus, atoms up to third nearest neighbors are included. Atoms on the third extra plane are beyond the cutoff range of the EAM potential and therefore are not necessary.

The boundary atoms experience an incomplete configuration of neighboring atoms. To avoid the relaxation of boundary atoms from their equilibrium positions,

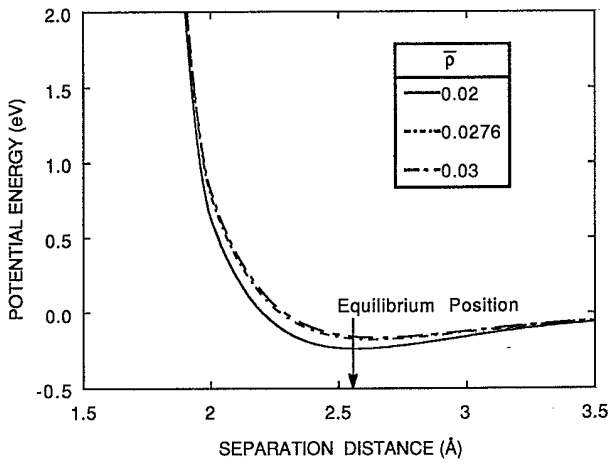

FIG. 1. Composite pair–many-body potential for copper as a function of the interatomic separation. The potential is shown for total average local electron density $\bar{\rho}$ of 0.02, 0.0276, and 0.03 Å^{-3}.

a balancing external force must be introduced. A spring constant is also introduced which allows boundary atoms to oscillate around their equilibrium positions. This spring constant k (a detailed derivation is given in the Appendix) is given by

$$k=\frac{El_0}{N_c} , \tag{4}$$

where E is the modulus of elasticity (Young's modulus), l_0 is the lattice constant, and N_c is the number of atoms in a unit cell. The equations of motion (EOM's) for boundary atoms are given by

$$\frac{\partial \mathbf{X}_i}{\partial t}=\mathbf{V}_i , \tag{5}$$

$$m_i\frac{\partial \mathbf{V}_i}{\partial t}=-\sum_{j,j\neq i}^{N}\nabla\phi_{ij}-\mu\mathbf{V}_i-k(\mathbf{X}_i-\mathbf{X}_{ie})+\mathbf{F}_b , \tag{6}$$

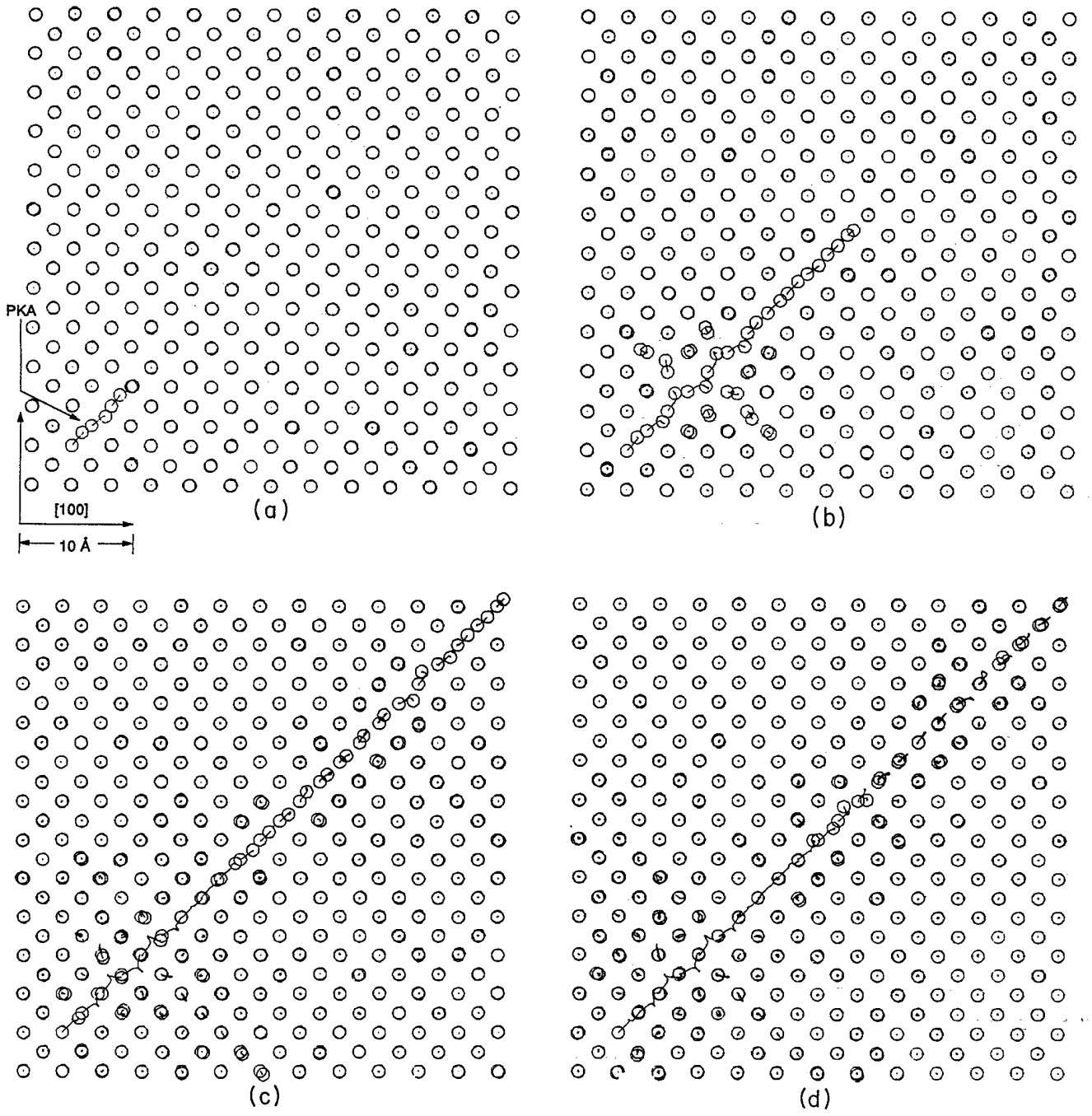

FIG. 2 Cascade trajectories at various times after the initiation of a 60-eV Cu PKA in copper at 300 K [$t=0.03$, 0.14, 0.29, and 0.50 ps for, respectively, (a)–(d)].

where $\mathbf{X}_i$ and $\mathbf{V}_i$ are the current position and velocity of particle i, ϕ_{ij} is the potential for particle j on i, $\mathbf{X}_{ie}$ is the equilibrium position, and $\mathbf{F}_b$ is the net balancing force. A damping constant μ is selected so that the damping time constant is greater than the cascade propagation time across the computational box. The main function of this fictitious force is to reduce the cascade energy reflection from cell boundaries.

The EOM's are integrated using Euler and leapfrog methods.[24,25] The time step is chosen to be small enough so that, within each integration step, interatomic forces and potentials are near constant for all particles in the system. This allows atoms in the Ziegler potential regime to move a small fraction of the screening length for each time step. The time step is therefore dynamically computed throughout the whole cascade simulation. A consequence of the use of dynamic time steps is that both the Euler and leapfrog methods are accurate only to first order.

IV. RESULTS

Figure 2 shows atomic trajectories at different times after the initiation of a 60-eV Cu PKA in copper along the [110] direction in a (001) plane at 300 K. The initial and ending positions of lattice atoms are marked by open circles. Their trajectories in between are connected using line segments. In this figure we do not show boundary atoms for clarity of demonstration. The figure shows that the length of the linear replacement collision sequence (RCS) reaches its final value after ~0.15 ps. A linear replacement chain of 10.5 displaced atoms, the equivalent of a net displacement of about 25 Å along the [110] direction, is produced. The initial speed of the PKA is 135 Å/ps. The average kinetic energy available for the RCS is about half of the initial PKA energy. The average speed is about 95 Å/ps. If the subsequent slowing down of the RCS is considered, it is clear that the propagation speed of the RCS is faster than can be explained by the speed derived from the kinetic energy alone.

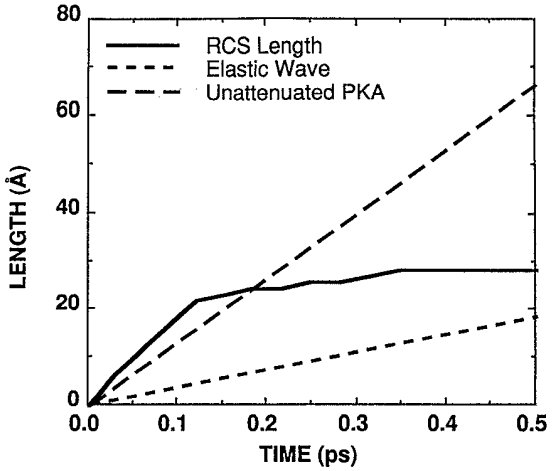

FIG. 4. Comparison of RCS propagation with those of a longitudinal elastic (sound) wave and the initial PKA.

Figure 3 shows the total energy for the same 60-eV cascade as a function of time. The total energy of the system starts at about 160 eV, which includes 60 eV of PKA energy; the balance represents the thermal energy content of the system of particles. The energies displayed in Fig. 3 are divided up into kinetic and potential components to show the exchange of these components as the cascade slows down. The total system energy remains constant until boundary effects become significant at about 0.3 ps. Beyond that time, a fraction of the cascade energy is dissipated in boundary regions. It is also shown that the exchange of potential and kinetic energies occurs on a time scale of about 0.05 ps.

Figure 4 shows the propagation of RCS and the longitudinal elastic (sound) wave as functions of time. Also included is the expected position of the PKA if we assume that its energy is not dissipated in the cascade and that it is free streaming at the initial speed. The propagation of

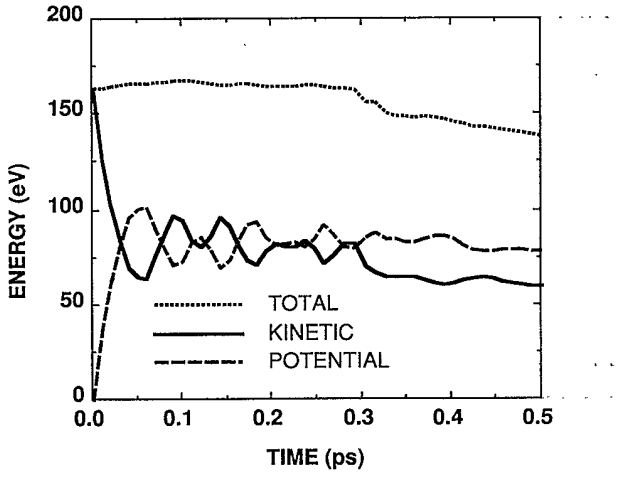

FIG. 3. Total, kinetic, and potential energies as functions of time for a collision cascade induced by a 60-eV Cu PKA in copper.

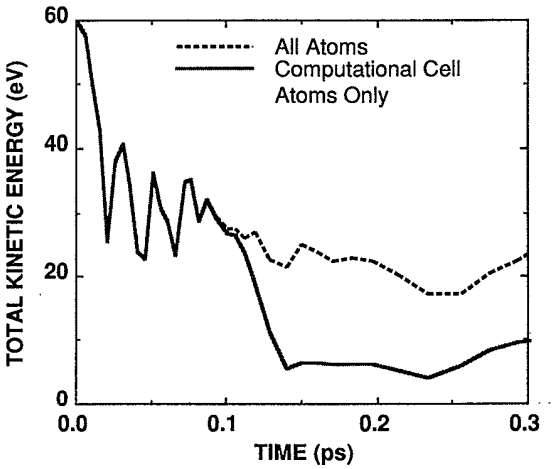

FIG. 5. Kinetic-energy partitioning as a function of time for the collision cascade.

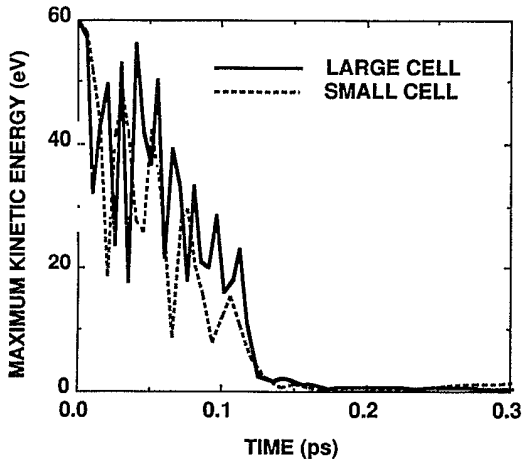

FIG. 6. The maximum kinetic energy associated with any of the atoms during the collisional phase of cascade evolution initiated by a 60-eV Cu PKA in copper.

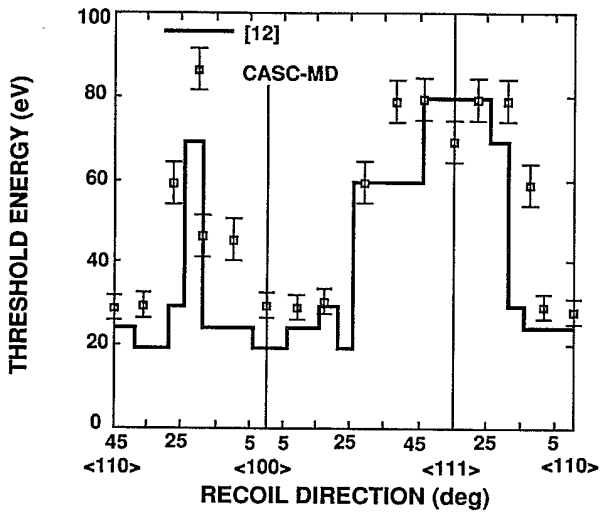

FIG. 8. Comparison between calculated displacement threshold energies along different directions at 10 K, and experimental data of King and Benedek (Ref. 12). A defect resistivity value $\sim 2.8\times 10^{-4}$ Ω cm is used in obtaining the experimental data.

the RCS clearly indicates that, in near-displacement-threshold interactions, focused collision sequences subside very fast (on a time scale of about 0.1 ps). The speed of cascade-energy propagation is much faster than the average thermal phonon (sound) speed. The longitudinal elastic wave speed v_s is calculated for isotropic copper using the relationship[26]

$$v_s=\sqrt{E/\rho}\ , \tag{7}$$

where E is the modulus of elasticity and ρ is the specific density for copper. The speed of cascade-energy propagation is also faster than the speed of higher-order knock-on atoms. The collective motion of participating atoms in a linear RCS through the simultaneous potential field is responsible for this propagation speed. The many-body interaction helps in this collective motion because of its long-range nature.

Figure 5 shows the total cascade kinetic energies for all of the atoms in the simulation system (including boundary atoms) and for the atoms in the computational cell only (excluding boundary atoms) for the same 60-eV cascade. It can be seen that boundary atoms are not influenced by the existence of a collision cascade until the end of the collisional phase. Therefore, the total system energy remains unchanged until the cascade energy reaches the boundary. The total system energy for the computational cell decreases because a fraction of the energy is channeled into the boundary atoms. This behavior also ensures that there is no energy reflection to interfere with the cascade dynamics and indicates that the selected size of the computational cell is adequate.

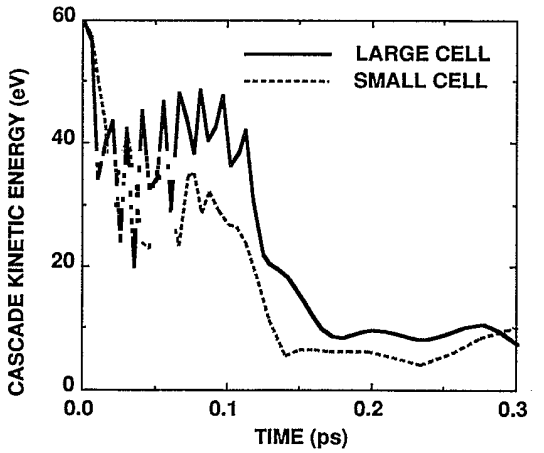

FIG. 7. Cascade kinetic energies as functions of time for two computational cell sizes.

Figure 6 shows the maximum kinetic energy associated with any of the recoils in two computational cell sizes (545 and 1301 atoms) for the same 60-eV collision cascade. Both simulations show that the duration of the collisional phase is approximately 0.15 ps. The kinetic energy of any of the atoms, at the end of this collisional phase, is well below the energy necessary to cause an atomic displacement. Figure 7 shows the cascade kinetic energy for two computational cell sizes. The cascade kinetic energy for the larger computational cell is summed over atoms which correspond to those in the smaller computational cell. At 300 K, the initial thermal energy content in the small computational cell is about 20 eV. Near thermalization is achieved at the end of the kinetic phase.

In Fig. 8, we compare the results of our calculations to the experimental measurements of King and Benedek[12] on copper at 10 K. Our simulations indicate that, while the displacement threshold energy is around 20 eV for copper, substantially larger energy is needed to displace copper atoms along the [111] and between [110] and [100] directions. Our calculations are quite consistent with the experiments of King and Benedek[12] who used a defect resistivity value of $\sim 2.8\times 10^{-4}$ Ωm cm to obtain the displacement threshold surface.

V. CONCLUSIONS

This study of the collisional phase of low-energy cascade evolution shows the following: (1) The development of a replacement collision sequence, which leads to a stable Frenkel pair, is completed in about 0.1 ps. (2) The initial propagation of a RCS is much faster than the longitudinal elastic (sound) wave in copper and is even faster than the initial PKA speed, showing that cascades propagate through collective atomic motions. (3) The close agreement of our MD results with the experimental data on the displacement threshold surface indicates the usefulness of this composite potential for the simulation of low-energy ion-solid interactions.

ACKNOWLEDGMENTS

This work was supported by the U.S. Department of Energy, Office of Fusion Energy, Grant No. DE-FG03-84ER52110, with the University of California, Los Angeles.

APPENDIX

The spring constant k is derived as follows. The uniaxial stress-strain relation is given by

$$\sigma = E\epsilon \ ,$$

where σ is the stress, E is the modulus of elasticity, and ϵ is the strain, given by $\sigma = F/A$ and $\epsilon = \delta l / l$, where F is the force, A is the area where the force is exerted, l is the length, and δl is the elongation. Considering a slab of unit area, and a length of a lattice constant l_0, we can rewrite the first equation as

$$F = E\frac{\delta l}{l_0} \ .$$

The total number N_a of atoms contained in this slab is

$$N_a = \frac{V}{l_0^3} N_c = \frac{(1) l_0}{l_0^3} N_c = \frac{N_c}{l_0^2} \ ,$$

where N_c is the number of atoms in a unit cell. The last two equations yield the force per atom f as

$$f = \frac{F}{N_a} = \frac{E l_0 \delta l}{N_c} = k \delta l \ .$$

The "equivalent" spring constant is then given by

$$k = \frac{E l_0}{N_c} \ .$$

[1]M. Yoshida, J. Phys. Soc. Jpn. **16**, 44 (1961).
[2]O. Oen and M. T. Robinson, J. Appl. Phys. **34**, 2515 (1964).
[3]T. Ishitani, R. Shimuzu, and K. Murata, Jpn. J. Appl. Phys. **11**, 125 (1972).
[4]H. L. Heinisch, J. Nucl. Mater. **103-104**, 1325 (1981); also, J. Nucl. Mater. **117**, 46 (1983).
[5]S. P. Chou and N. M. Ghoniem, J. Nucl. Mater. **117**, 55 (1983).
[6]J. B. Gibson, A. N. Goland, M. Milgram, and G. H. Vineyard, Phys. Rev. **120**, 1229 (1960).
[7]J. R. Beeler, Jr., Phys. Rev. **150**, 470 (1966).
[8]R. N. Stuart, N. W. Guinan, and B. J. Borg, Radiat. Eff. **30**, 129 (1976).
[9]J. D. Schiffgen and R. D. Bourquin, J. Nucl. Mater. **69-70**, 790 (1978).
[10]A. Tenenbaum and N. V. Doan, J. Nucl. Mater. **69-70**, 775 (1978).
[11]T. Diaz de la Rubia, R. S. Averbeck, and H. Hsieh, J. Mater. Res. **4**, 579 (1989).
[12]W. E. King and R. Benedek, Phys. Rev. B **23**, 6335 (1981).
[13]W. E. King and R. Benedek, in *Point Defects and Defect Interactions in Metals*, edited by J. Takamura, M. Doyama, and M. Kiritini (University of Tokyo Press, Tokyo, 1982), p. 789.
[14]W. E. King and R. Benedek, J. Nucl. Mater. **117**, 26 (1983).
[15]M. S. Daw and M. I. Baskes, Phys. Rev. Lett. **50**, 1285 (1983).
[16]M. S. Daw and M. I. Baskes, Phys. Rev. B **29**, 6443 (1984).
[17]S. M. Foiles, Phys. Rev. B **32**, 7685 (1985).
[18]S. M. Foiles, M. I. Baskes, and M. S. Daw, Phys. Rev. B **33**, 7983 (1986).
[19]P. Hohenberg and K. Kohn, Phys. Rev. **136**, B864 (1964).
[20]R. A. Johnson, Phys. Rev. B **37**, 3924 (1988).
[21]D. J. Oh and R. A. Johnson, J. Mater. Res. **3**, 471 (1988).
[22]J. F. Ziegler, J. P. Biersack, and U. Littmark, *The Stopping and Range of Ions in Solids* (Pergamon, New York, 1985), p. 48.
[23]E. Clementi and C. Roetti, At. Nucl. Data Tables **14**, 177 (1974).
[24]D. E. Potter, *Computational Physics* (Wiley, London, 1973), p. 37.
[25]H. L. Berk and K. V. Roberts, in *Methods in Computational Physics*, edited by B. Alder, S. Fernbach, and M. Rotenberg (Academic, New York, 1970), Vol. 9, p. 111.
[26]M. Alonso and E. J. Finn, *Physics* (Addison-Wesley, Reading, MA, 1970), p. 534.